FIELD AND ANALYTICAL EXAMINATION OF NEAR-SURFACE FACETS

Andrew E. Slaughter* and Edward E. Adams
Department of Civil Engineering, Montana State University, Bozeman, MT

ABSTRACT: North- and south-facing field research locations were established that included meteorological stations coupled with daily observations and grain-scale images of the upper few centimeters of the snowpack. In three seasons, 47 near-surface facet events at the south-facing station were recorded. Statistical analysis of these events indicated two factors were related to facet formation: incoming short-wave radiation and relative humidity. Using a thermal model, variance-based sensitivity analysis, and Monte Carlo simulations the environmental conditions and snow material properties that lead to radiation-recrystallization were explored analytically. Based on the presence of specific temperature profiles that are understood to lead to facets, eight terms were determined to be influential in facet formation, which were further reduced to thermal conductivity and a dimensionless term, Ω, defined as the ratio of absorbed short-wave to long-wave radiation. Using these parameters, a graphical means for predicting the presence of near-surface facets is presented. Predicting the presence of near-surface facets may be possible with meteorological and basic snowpack information.

KEYWORDS: Near-surface Facets, Radiation Recrystallization, Heat-Transfer Model, Sensitivity Analysis, Monte Carlo Simulations

1. INTRODUCTION

Near-surface facets are a common weak-layer leading to slab avalanches (Schweizer and Lutschg, 2001). Research discussing the conditions necessary for producing this layer is widespread and ranges from field studies (Colbeck and Jamieson, 2006; McCabe et al., 2008) to laboratory investigations (Morstad et al., 2007) to studies linking the two (Slaughter et al., 2009). Additionally, computer models continue to increase in accuracy for both predicting weak-layers and stability (Lehning et al., 2004) and visualizing the spatial variability of the snowpack (Staples et al., 2006; Adams et al., 2009, 2010).

The overall goal of the work presented here, which is a portion of the work performed by Slaughter (2010), is to improve the current understanding of radiation-recrystallization and develop a useful tool to aid in the prediction of facet formation. This was accomplished by (1) compiling three seasons of weather data and field observations, (2) using statistical analysis and a 1-D thermal model to explore a range of environmental conditions not possible in the field, and (3) utilizing Monte Carlo simulations to quantify the conditions likely to lead to facet formation.

* *Corresponding author address:* Andrew E. Slaughter, 205 Cobleigh Hall, Montana State University, Bozeman, MT 59717; tel: 406-219-1133; fax: 406-994-6105; email: andrew.e.slaughter@gmail.com

2. METHODS

2.1. Field Study

Two study plots were selected—a north- and a south-facing slope—on Pioneer Mountain at the Yellowstone Club (YC) near Big Sky, Montana. These sites have been used in previous research endeavors (Cooperstein et al., 2004; Staples et al., 2006; Adams et al., 2009; Slaughter and Adams, 2009; Slaughter et al., 2009; Adams et al., 2010; Slaughter, 2010), and were similarly instrumented to measure a variety of environmental conditions. Also, the YC Ski Patrol maintained daily visual and written observations in addition to grain-scale images detailing the upper 5 cm of the snowpack. A detailed description of the weather stations, instrumentation, and observations was presented in Slaughter (2010). For the results presented here six parameters from the south-facing slope are considered: incoming short-wave (SW) and long-wave (LW) radiation, air temperature (T_a), snow surface temperature (T_s), wind speed (V_w), and relative humidity (RH).

2.2. Numerical Analysis

A statistical approach—the SOBOL method of sensitivity analysis (Saltelli, 2002)—was utilized to explore radiation recrystallization. Complete details of the methods were given by Slaughter (2010). This sensitivity analysis quantifies how much the

variance of each input contributes to the total variance of the model output. This methodology required hundreds of thousands of model evaluations; as such, a computationally efficient model is required.

A modified version (see Slaughter, 2010) of the 1-D model originally implemented by Morstad et al. (2007) was utilized for the analysis. During model evaluations all parameters remained constant, except short-wave radiation which was varied as a sine-wave. The 11 input parameters explored here are listed in Table 1; the symbols and *i*-reference index in this table are used throughout the remainder of this paper. The model simulated 10 hours from sunrise to sundown and all inputs were allowed to vary independently, a requirement of the method.

Table 1: List of thermal model input parameters explored using sensitivity analysis.

i	*Sym.*	*Name*	*Units*
1	ρ	Snow density	kg/m^3
2	k	Thermal conductivity	W/(m· K)
3	C_p	Specific heat	kJ/(kg· K)
4	T_s^{int}	Initial snow temperature	°C
5	κ	Extinction coefficient	m^{-1}
6	*LW*	Incoming long-wave rad.	W/m^2
7	*SW*	Incoming short-wave rad.	W/m^2
8	α	Albedo	
9	V_w	Wind speed	m/s
10	T_a	Air temperature	°C
11	*RH*	Relative humidity	%

The analysis required that each input be fitted to a continuous distribution function, from which the data was sampled at random. The first five input parameters were assigned uniform distributions based on data published by Armstrong and Brun (2008) as summarized in Table 2. The remaining six parameters were assigned distributions associated with recorded field data. The field data was acquired from the south-facing station during the 2009/2010 season. The distributions were based on mean daily values of short- and long-wave radiation, wind speed, air temperature, and relative humidity. The initial snow temperature was assigned a value at sunrise. Table 2 summarizes these distribution sets, which were developed using EasyFit 5.4 (Mathwave Technologies). The best-fitting distribution, based on the Kolmogorov-Smirnov test (Massey, 1951), that was also available in MATLAB (The Mathworks, Inc.) was selected. In all cases, it may be stated that at the 10% confidence level the raw data was from the same distribution as presented in Table 2, as indicated by the *p*-values listed (i.e., each was less than 0.1). Figure 1 includes a comparison of the recorded data (histograms) with the fitted probability density functions.

Table 2: Continuous distribution functions for model input parameters. The parameters (a,b,c) are ordered as defined in the MATLAB documentation (MATLAB, 2010), where gev = generalized extreme value, unif = uniform, and norm = normal.

Snow Properties			*Atmospheric Properties*					
Sym.	*Min.*	*Max.*	*Sym.*	*Type*	*a*	*b*	*c*	*p*-value
ρ	50	500	T_s^{int}	gev	-0.562	3.186	-6.844	0.066
k	0.1	0.7	*LW*	gev	-0.422	32.55	246.2	0.063
c_p	1795	2115	*SW*	unif	26.68	794.0		0.084
α	0.4	0.95	V_w	gev	-0.0219	0.420	1.35	0.078
κ	40	200	T_a	norm	-4.30	4.01		0.058
			RH	gev	-0.532	18.14	57.41	0.054

A single output was examined, the "knee" temperature gradient (TG_K), which is characteristic of what would likely form due to solar penetration (subsurface warming) and surface radiative cooling, which is typically associated with radiation-recrystallization (Birkeland, 1998), as shown in Figure 2. For each model evaluation, if the "knee" was not present it was assigned a value of zero, otherwise the gradient was utilized.

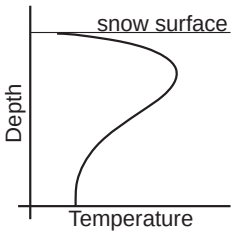

Figure 2: Schematic showing the "knee" temperature profile.

The extended SOBOL variance-based sensitivity method (Saltelli, 2002) quantifies the contribution of the variance of each input parameter (see Table 1), including interactions between parameters, to the total variance of the model output. A sampling size of 15,000 replicates was utilized, resulting in 360,000 model runs to apply the SOBOL method. The 90% confidence intervals were calculated using bootstrap BCa method (Efron and Tibshirani, 1993) with 10,000 re-samplings of the aforementioned model runs. The results discussed include four terms: the first-order index S_i gives the contribution of the i^{th} input parameter; the second-order index $S_{i,j}$ gives the contribution due to interaction between i^{th} and j^{th} terms; a higher-order index S_i^h, which includes all interactions greater than second-order; and the total-effect index S_i^T provides the contribution of the i^{th} parameter and all associated interactions to the k^{th} order (e.g., $S_1^T = S_1 + S_{1,2} + S_{1,3} + ... + S_i^h$). The *i* and *j* subscripts refer to the numbers in Table 1.

3. RESULTS

3.1. Field Study

During three winter seasons—07/08, 08/09, and 09/10—47 near-surface facet events were recorded.

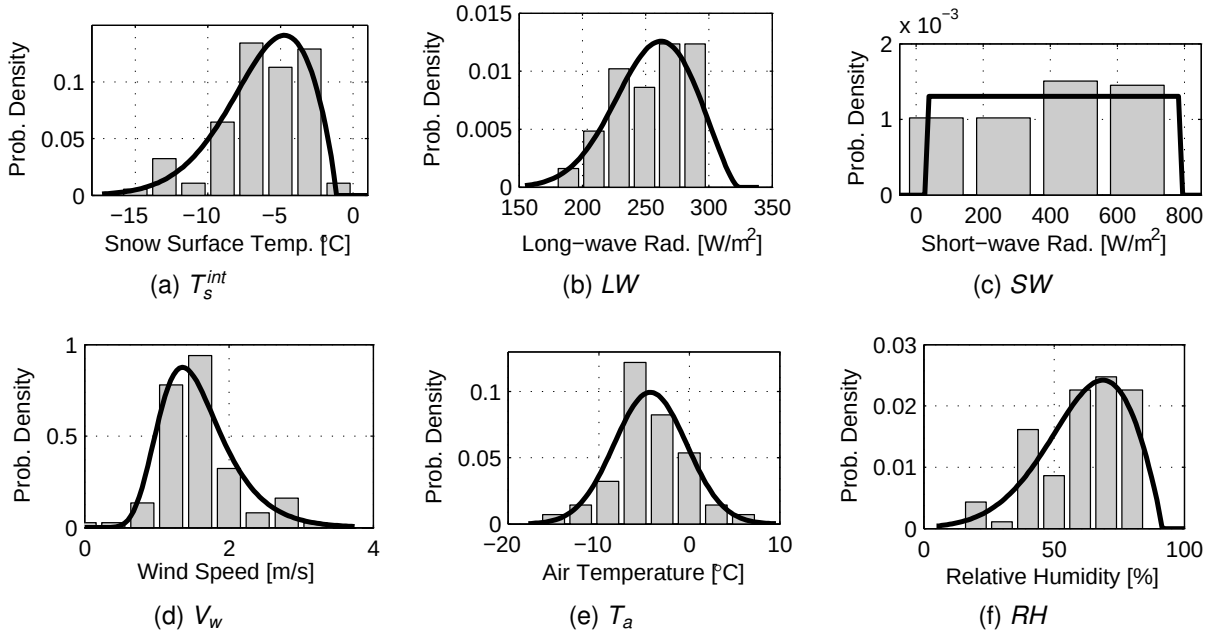

Figure 1: Comparison of the 09/10 season raw data (histograms) with the fitted probability distribution functions (lines) presented in Table 2; the distributions were used as the basis for the sensitivity analysis.

These events occurred exclusively at the south weather station. An event was defined by two criteria: (1) the field notes must identify the crystals as near-surface facets and (2) the images must corroborate the field note statements. Detailing each of the events is impractical, but further details are included in Slaughter et al. (in review) and Slaughter (2010). The results are summarized in Figure 3, which contains the daily mean averages of all recorded days compared to the event specific days.

A statistical comparison—a two-sample Kolmogorov-Smirnov test (Massey, 1951)—was used to determined if the events were from the same distribution as the complete set of weather data. If the distributions were distinct then the events were not a random sample of the entire data set, thus it was assumed the parameter may have been important to facet formation. The results from the test, at the 5% significance level, indicated that only two parameters may have been linked to the formation of near-surface facets: short-wave radiation and relative humidity. Drawing specific conclusions from this data was difficult, which motivated the numerical methodology (see Section 2.2) used that allows for a nearly infinite set of environmental conditions to be explored. Nonetheless, some generalizations may be made visually from the data in Figure 3, namely near-surface facets formed in the field with $SW > 500$ W/m^2, T_a between -10 and 0 °C, $T_s >$ -10 °C, $V_w < 2$ m/s, and $RH <$ 70%.

3.2. Numerical Analysis

The resulting total-effect indices as a function of model evaluation time for the "knee" temperature gradient is presented in Figure 4, which were normalized such that the sum of the individual indices was always 100%. During the middle of the evaluation, eight parameters influenced the gradient: ρ(1), k(2), κ(5), *LW*(6), *SW*(7), α(8), V_w(9), and T_a(10) (see Figure 5). The mid-day (five-hour mark of the model evaluations) is used herein to simplify the analysis; considering the relatively uniform temporal behavior of the sensitivity (Figure 4), it is likely a reasonable representation of the overall behavior.

Interestingly, two spikes were observed in Figure 4 at approximately the two- and eight-hour marks. This behavior was likely related to the thermal capacitance of the snow, or how "difficult" is it to change the temperature of the snow. Initially, the snow was being warmed by the incoming short-wave radiation, but depending on the values of ρ(1), c_p(3), and T_s(4) this warming was resisted at a rate governed by k(2). And to a greater extent, the opposite was observed near the end of the day, as the solar radiation decreased and the snow began to cool.

The total-effect indices were composed of first-, second-, and higher-order terms. Therefore, each total-effect index may be divided into parts, as shown in Figure 6 for k(2). The sum of the sensitivities for the bars in this figure equal the height of the S_2^T

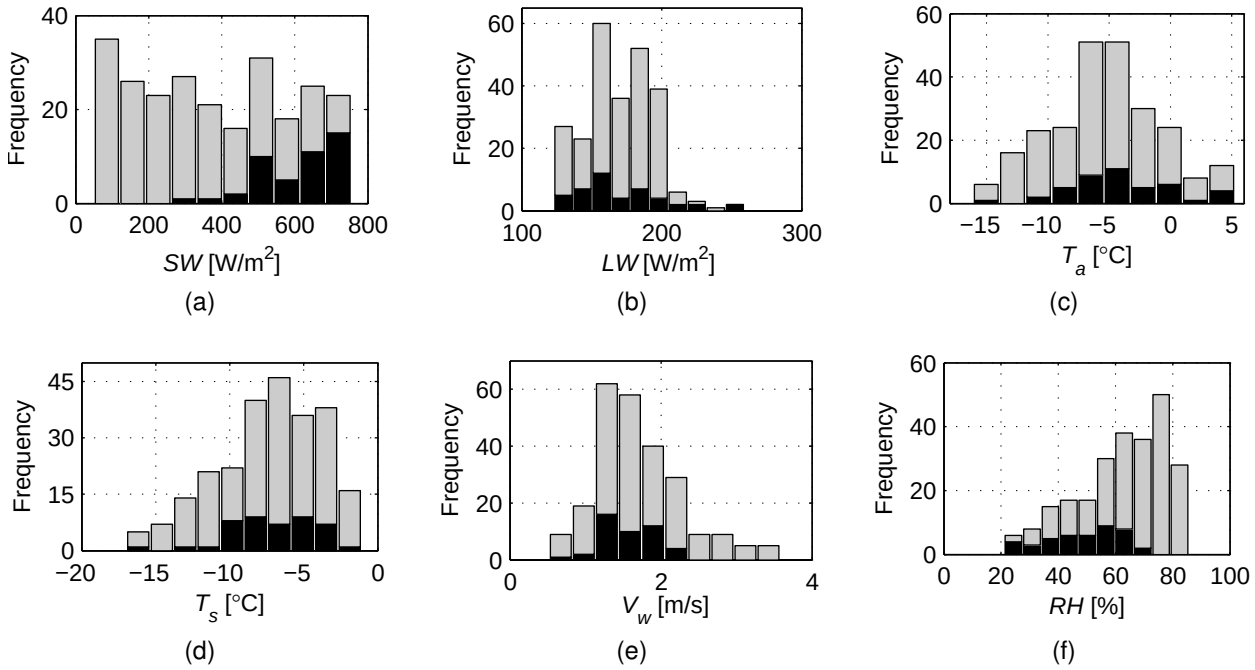

Figure 3: Histograms comparing all recorded daily average weather conditions (▬) to the days associated with observed near-surface facet events (■).

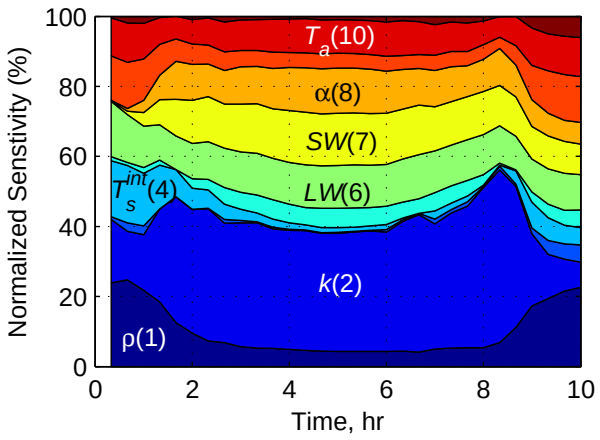

Figure 4: Stacked area chart of normalized total-effect indices for the "knee" temperature gradient (TG_K) as a function of evaluation time. The areas are stacked in order from top to bottom as listed in Table 1.

bar in Figure 5. In the case of $k(2)$, only three terms—considering the confidence intervals of the parameters—are non-zero: S_2, $S_{2,6}$, and S_2^h. When all of the results are considered (see Table 3), with the exception of S_2, higher-order terms (S_i^h) dominate the results. This indicated that, in general, only certain combinations of parameters led to the occurrence of a "knee" temperature gradient.

Based on the sensitivity analysis results it may be stated that $c_p(3)$, $T_s^{int}(4)$, and $RH(11)$ have negligible effect on TG_K, and thus may be excluded from further analysis; hence, $TG_K = f(\rho, k, \kappa, LW, SW, \alpha, V_w, T_a)$. With respect to developing a useful prediction tool, removing three parameters offers little help, so this relationship must be simplified further. Conductivity, $k(2)$, must be included since approximately 70% of the variance in TG_K may be attributed to it. Also, considering that the focus is on radiation recrystallization, $LW(6)$, $SW(7)$, and $\alpha(8)$ are a natural selection, especially when grouped into a dimensionless term,

$$\Omega = \frac{SW}{LW}(1-\alpha),$$

which is the ratio of absorbed short-wave to long-wave radiation. In the analysis presented in the following section, the remainder of the terms—$\rho(1)$, $\kappa(4)$, $V_w(9)$, and $T_a(10)$—are neglected. This is not unreasonable considering the sensitivity analysis results that indicated all except $k(2)$ were dominated by higher-order terms; therefore any influences in the neglected terms are likely coupled to changes in the terms considered, thus indirectly accounted for. As such, the "knee" temperature gradient may be estimated as $TG_K \approx f(k, \Omega)$.

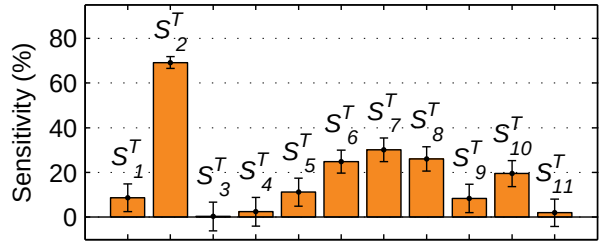

Figure 5: Total-effect indices (S^T) for the "knee" temperature gradient (TG_K) at mid-day.

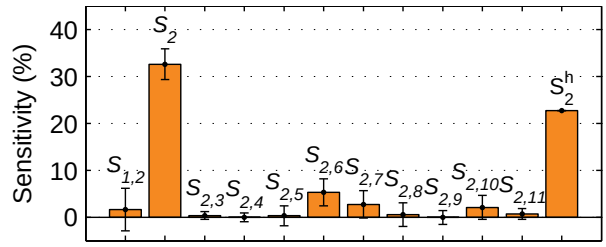

Figure 6: First-, second-, and higher-order sensitivity indices for $k(2)$ based on the TG_K results at mid-day.

Table 3: Sensitivity analysis results from TG_K at mid-day. The diagonal provides the first-order indices, the off-diagonal the second-order indices, and the higher-order and total-effect are listed in the bottom two rows. Non-zero terms, based on the associated confidence intervals, are given in bold.

i \ j	1	2	3	4	5	6	7	8	9	10	11
1	0.3	1.6	0.1	-0.1	0.1	-0.1	-0.1	0.2	-0.1	-0.2	0.1
2	1.6	**32.6**	0.4	0.0	0.3	**5.3**	2.8	0.6	-0.0	2.1	0.7
3	0.1	0.4	-0.0	-0.0	0.0	0.0	0.1	-0.0	-0.0	-0.1	0.0
4	-0.1	0.0	-0.0	-0.1	0.2	0.4	0.1	0.2	0.1	0.2	0.2
5	0.1	0.3	0.0	0.2	**1.9**	0.1	-0.1	-0.1	0.1	-0.2	0.1
6	-0.1	**5.3**	0.0	0.4	0.1	**3.2**	0.6	0.6	0.2	0.4	0.3
7	-0.1	2.8	0.1	0.1	-0.1	0.6	**1.9**	**2.1**	-0.1	-0.4	-0.4
8	0.2	0.6	-0.0	0.2	-0.1	0.6	**2.1**	**1.2**	-0.4	-0.3	0.2
9	-0.1	-0.0	-0.0	0.1	0.1	0.2	-0.1	-0.4	0.1	0.8	0.6
10	-0.2	2.1	-0.1	0.2	-0.2	0.4	-0.4	-0.3	0.8	**2.5**	0.2
11	0.1	0.7	0.0	0.2	0.1	0.3	-0.4	0.2	0.6	0.2	-0.0
Higher	6.8	22.8	-0.2	1.3	8.8	13.7	23.5	21.8	7.2	14.5	-0.1
Total	**8.7**	**69.1**	0.3	2.4	**11.2**	**24.8**	**30.0**	**26.0**	**8.4**	**19.5**	2.0

4. ANALYSIS AND DISCUSSION

The results from the field data (Section 3.1) provided some generalization about the conditions that lead to radiation recrystallization and the sensitivity analysis (Section 3.2) yielded quantification of the most influential parameters on the formation of the "knee" temperature gradient that is known to lead to near-surface facet formation. The final task was to specifically quantify the conditions that lead to facets and build a tool for predicting formation. To accomplish this the model evaluations from the SOBOL analysis, which are a set of Monte Carlo simulations, were utilized to further quantify the conditions by separating the portion of the input parameters leading to a specific output. For example, the levels of long-wave radiation that correspond to high temperature gradients.

In this case, the output was a range for "knee" temperature gradient that may to lead to near-surface facet formation in a single day: 200–600 °C/m. Values reported in the literature range from approximately 100–600 °C/m (Fukuzawa and Akitaya, 1993; Hardy et al., 2001; Morstad et al., 2007; Slaughter et al., 2009). Morstad et al. (2007) indicated that gradients on the order of 100 °C/m may be inadequate (Exp. #8). One experiment is of little value for making such a claim, but this statement gains credibility considering the work of Pinzer and Schneebeli (2009), which provides additional evidence that on time scales of less than a day "temperature gradients on the order of 100 °C/m do not lead necessarily to faceting…." Considering that the simulations presented here only spanned 10 hours, a lower limit of 200 °C/m was assumed to be necessary for facet formation to occur. The upper limit was assumed to remain at 600 °C/m. Values larger than this were assumed to be unrealistic.

Using this defined range of TG_K the 360,000 model evaluations were reduced to a subset of 32,937 evaluations, which indicated that 9.1% of the model evaluations resulted in conditions favorable for radiation recrystallization. For comparison, the field data resulted in 47 events out of 249 observations (18.8%). Figure 7(a) is a scatter plot showing the relationship of Ω and k for the TG_K limited subset.

This subset was used to define highest density regions (HDRs) that surround the raw data in Figure 7(a) (Hyndman, 1996). An HDR is produced from a multivariate (Ω and k) probability density function, which was created using the normal product kernel (Martinez, 2008), resulting in the distribution shown in Figure 7(b). The HDRs were generated by slicing a plane through Figure 7(b). For example, the 95% HDR was sliced such that 95% of the raw data has a probability density greater than the data outside of the region. Hence, it may be stated that in a random set of observations from within the population, 95% are expected in the defined region.

Based on the computed distribution in Figure 7(b), 95%, 68%, 32%, 20%, and 10% HDRs are defined, as shown in Figure 8. These ranges were selected because they were approximately proportional to confidence levels typically associated with a normal distribution. And, if the data was normally distributed these HDRs would be equivalent to 2σ, 1σ, $\frac{1}{2}\sigma$, $\frac{1}{4}\sigma$, and $\frac{1}{8}\sigma$ confidence regions.

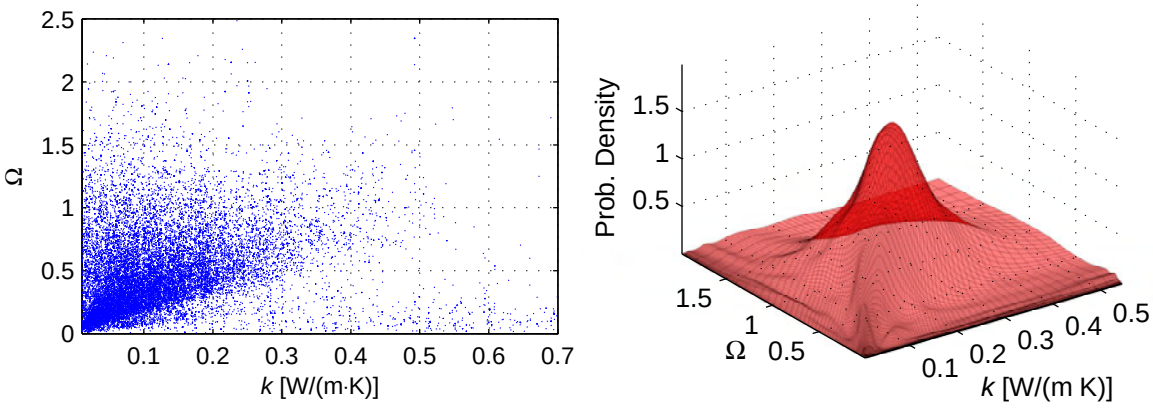

Figure 7: Scatter plot (a) and multivariate probability density function (b) of Ω and k with TG_K limited from 200–600 °C/m.

It is important to explain that the TG_K limited subset does not limit the data in any other way. That is, the variance of all 11 parameters is inherit. For this reason, the assumption that the higher order interactions of the neglected terms—ρ, κ, V_w, T_a—are accounted for in Ω and k is reasonable (see Section 3.2). For illustration, consider the following hypothetical example: Ω = 1 and k = 0.1 W/(m·K) may only result in a TG_K between 100–600 °C/m if T_a is less than -5°C and V_w = 1 m/s, but not if V_w is any other value. The data presented in Figure 7 accounts for such situations, but does not allow for specific quantification.

Included in Figure 8 are the laboratory results presented by Morstad et al. (2007) and Slaughter et al. (2009) as well as the field data discussed in this paper and detailed further in Slaughter et al. (in review). The field data is presented as a region due to the lack of measurements for α and k. Based on estimates detailed by Slaughter (2010, Ch. 10) the recorded events likely lie somewhere in the region defined. Using the HDRs it is possible to examine the fit of the specific points, e.g., 95% of the data should fall within the outermost ring. Of the 16 points, 15/16 (94%), 12/16 (75%), 6/16 (38%), 5/16 (31%), and 2/16 (13%) are within the 95%, 68%, 32%, 20%, and 10% HDRs, respectively. Considering the limited number of points, that the experiments were not conducted using a robust experimental design, and the overlap of the field data region the apparent agreement is a promising result. Figure 8 demonstrates the potential for numerical explorations to lead to usable tools for predicting metamorphism based solely on the environmental conditions. The region defined by the 32% HDR is presented as a postulate as the "optimum" region for near-surface facet formation on south-facing slopes in Southwest Montana; however, further validation and exploration is required before end-user predictive tools may be developed and extrapolated to other geographical regions.

5. CLOSING REMARKS

The primary objective of this paper was to present a tool for assessing near-surface faceting due to radiation-recrystallization, which was accomplished to some respect with Figure 8. This figure relates the non-dimensional term Ω to thermal conductivity (k). Based on the numerical simulations performed a graphical tool is proposed for further exploration that defines ideal conditions that lead to strong temperature gradients (200–600 °C/m)—those conducive to radiation recrystallization—that relies solely on radiation-related terms and thermal conductivity.

The research presented here is only a small portion of the analysis conducted and only scratches the surface of the possibilities for such analysis. The results indicate the potential to use purely numerical methods to gain an understanding of the environmental conditions that lead to the formation of near-surface facets and weak-layers in general. Future analysis already underway includes the analysis of layered snowpacks, contaminated layers, and various initial conditions and input data sets that will inevitably expand upon the data given here. The authors believe that similar analysis should be conducted using more detailed models that include micro-structural components such as SNOWPACK.

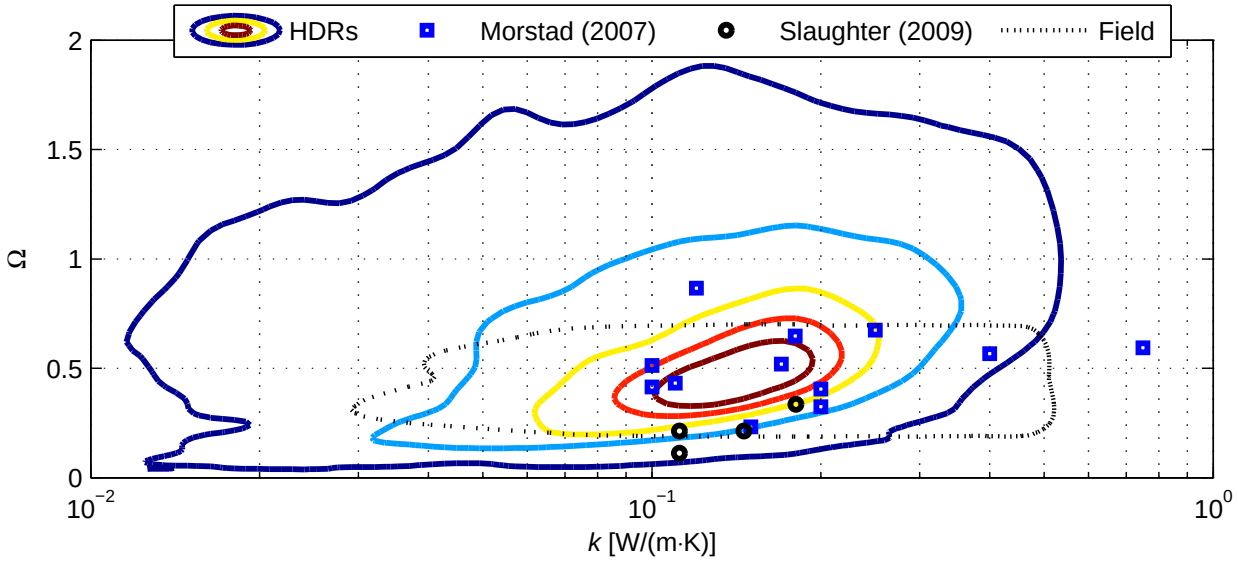

Figure 8: Graph of 95% (outer), 68%, 38%, 20%, and 10% (inner) HDRs for the TG_K limited from 200–600 °C/m.

6. ACKNOWLEDGMENTS

A portion of this work was conducted at the Montana State University Subzero Science and Engineering Research Facility, which was developed with the support of the National Science Foundation (NSF) Grant #ANT-0521360 and Murdock Charitable Trust. A portion of this work was funded by NSF Grant #EAR-0635977, the NSF Graduate Teaching Fellows in K–12 Education Program, and research grants from the 2000 International Snow Science Workshop and the American Avalanche Association.

7. REFERENCES

Adams, E., A. Slaughter, L. McKittrick, and D. Miller, 2010: The coupling of snow near surface metamorphism and surface energy balance in complex alpine terrain. *International Symposium on Snow, Ice and Humanity in a Changing Climate*, Sapporo, JP.

Adams, E., et al., 2009: Modeling variation of surface hoar and radiation recrystallization across a slope. *International Snow Science Workshop*, Davos, CH.

Armstrong, R. and E. Brun, 2008: *Snow and Climate: Physical Processes, Surface Energy Exchange, and Modeling*. Cambridge University Press.

Birkeland, K., 1998: Terminology and predominant processes associated with the formation of weak layers of near-surface faceted crystals in the mountain snowpack. *Arctic and Alpine Research*, **30 (2)**, 193–199.

Colbeck, S. and B. Jamieson, 2006: Surface hoar growth from valley clouds. *International Snow Science Workshop*, Telluride, CO.

Cooperstein, M., K. Birkeland, and K. Hansen, 2004: The effects of slope aspect on the formation of surface hoar and diurnally recrystalized near-surface faceted crystals: Implications for avalanche forecasting. *International Snow Science Workshop*, Jackson Hole, WY.

Efron, B. and R. J. Tibshirani, 1993: *An introduction to the Boostrap*. Chapman and Hall.

Fukuzawa, T. and E. Akitaya, 1993: Depth-hoar crystal growth in the surface layer under high temperature gradient. *Annals of Glaciology*, **18**, 39–45.

Hardy, D., M. W. Williams, and C. Escobar, 2001: Near-surface faceted crystals, avalanches and climate in high-elevation, tropical mountains of Boliva. *Cold Regions Science and Technology*, **33**, 291–302.

Hyndman, R., 1996: Computing and graphing highest density regions. *The American Statistician*, **50 (2)**, pp. 120–126.

Lehning, M., C. Fierz, B. Brown, and B. Jamieson, 2004: Modeling snow instability with the snow-cover model snowpack. *Annals of Glaciology*, **38 (1)**, 331–338.

Martinez, A., 2008: *Computational Statistics Handbook with MATLAB*. 2d ed., Chapman & Hall/CRC, Boca Raton, FL.

Massey, F., 1951: The Kolmogorov-Smirnov test for goodness of fit. *Journal of the American Statistical Association*, **46 (253)**, 68–78.

MATLAB, 2010: *MATLAB 2010a Documentation*. Natick, MA, The Mathworks, Inc.

McCabe, D., et al., 2008: Near-surface faceting on south aspects in Southwest Montana. *International Snow Science Workshop*, Whistler, B.C., 147–154.

Morstad, B., E. Adams, and L. McKittrick, 2007: Experimental and analytical study of radiation-recrystallized near-surface facets in snow. *Cold Regions Science and Technology*, **47 (1–2)**, 90–101.

Pinzer, B. and M. Schneebeli, 2009: Snow metamorphism under alternating temperature gradients: Morphology and recrystallization in surface snow. *Geophysical Research Letters*, **36 (23)**, L23 503.

Saltelli, A., 2002: Making best use of model evaluations to compute sensitivity indices. *Computer Physics Communications*, **145**, 280–297.

Schweizer, J. and M. Lutschg, 2001: Characteristics of human-triggered avalanches. *Cold Regions Science and Technology*, **33**, 147–162.

Slaughter, A., 2010: Numerical analysis of conditions necessary for near-surface snow metamorphism. Ph.D. thesis, Montana State University.

Slaughter, A. and E. Adams, 2009: Numerical investigation of factors causing near-surface metamorphism. *International Snow Science Workshop*, Davos, CH.

Slaughter, A., et al., 2009: An investigation of radiation-recrystallization coupling laboratory and field studies. *Cold Regions Science and Technology*, **59 (2–3)**, 126–132.

Slaughter, A., et al., in review: Field investigation of near-surface metamorphism of snow, II: Near-surface facets and near-coincidence with surface hoar. *Journal of Glaciology*.

Staples, J., E. Adams, A. Slaughter, and L. McKittrick, 2006: Slope scale modeling of snow surface temperature in topographically complex terrain. *International Snow Science Workshop*, Telluride, CO, 806–814.